ELSEVIER

Marine Geology 157 (1999) 145–158

MARINE GEOLOGY
INTERNATIONAL JOURNAL OF MARINE GEOLOGY, GEOCHEMISTRY AND GEOPHYSICS

Petrogenesis of ferromanganese nodules from east of the Chagos Archipelago, Central Indian Basin, Indian Ocean

Ranadip Banerjee [a,*], Supriya Roy [b], Somnath Dasgupta [b], Subir Mukhopadhyay [b], Hiroyuki Miura [c]

[a] *Geological Oceanography Division, National Institute of Oceanography, Dona Paula, Goa 403004, India*
[b] *Department of Geological Sciences, Jadavpur University, Calcutta, 700032, India*
[c] *Department of Geology and Mineralogy, Faculty of Science, Hokkaido University, Sapporo, 060, Japan*

Received 28 May 1997; accepted 24 July 1998

Abstract

Deep-sea ferromanganese nodules occur over a large area and on many different sediment types of the Central Indian Basin, Indian Ocean. Selected samples were studied to determine their chemical and mineralogical compositions and microstructural features. Repeated laminations of variable thickness, alternately dominated by todorokite and vernadite, are characteristic of these nodules. These laminae show, on electron microprobe line scans, corresponding interlaminar partitioning of Mn–Cu–Ni and Fe–Co. The bulk chemical compositions of these nodules plot in both the hydrogenetic and early diagenetic fields on the Fe–Mn–(Ni + Cu + Co) ×10 ternary diagram. The binary diagram depicting the covariation of Mn + Ni + Cu against Fe + Co shows two distinct parallel regression lines, one delineated by nodules from terrigenous, siliceous ooze and siliceous ooze–terrigenous sediments and the other by nodules from red clay, siliceous ooze–red clay and calcareous ooze–red clay. An increasing diagenetic influence in the nodules with the nature of the host sediment types was observed in the sequence: terrigenous → siliceous ooze and red clay → siliceous/calcareous ooze–red clay. A negative correlation between Mn/Fe ratio and Co and a positive correlation between Mn/Fe ratio and (Ni + Cu) was established. The nodules show dendritic, laminated, and globular microstructures formed by primary growth of Fe–Mn oxide laminae. Depositional hiatuses in the primary microstructures indicate that the growth of these nodules was episodic. The oxide laminations show extremely complex growth patterns. Scattered biogenic remains and mineral grains acted as accessory 'seeds' for growth of oxide layers in addition to the main nuclei. None of the primary microstructures can be uniquely linked to a particular growth process or growth rate. Radial cracks, cutting across primary microstructures, are often filled by todorokite of a later generation. Post-depositional modifications of the nodules were largely controlled by accreted biogenic remains as indicated by their progressive dissolution with increasing depth from nodule surfaces, their pseudomorphic replacement by todorokite and the later growth of phillipsite and todorokite in the microfossil molds. The growth patterns of the in-filled oxides are often controlled entirely by the cavity-walls and are discordant with the primary growth fabric. Primary todorokite was recrystallized to coarser grains of different chemical composition. Later generation veins of todorokite cut across and chaotically disrupted primary laminae.

Keywords: petrogenesis; ferromanganese nodules; chemical composition; microstructure; biota; diagenesis

* Corresponding author. E-mail: banerjee@esnio.ren.nic.in

0025-3227/99/$ – see front matter
PII: S0025-3227(98)00156-X

1. Introduction

Voluminous data on the chemical characteristics, growth processes, and growth histories, including growth rates, of deep-sea ferromanganese nodules from the world oceans are available in the literature, although integration of those data with petrographic evidence is rather limited. In an earlier study such an attempt was restricted to a few nodules from the siliceous ooze and red clay sediment provinces at two locations in the Central Indian Basin (CIB) (Roy et al., 1990). Interpretation of data obtained from that study refuted the specific correlation of microstructures to genetic processes deduced from Pacific nodules and the nodules studied by Roy et al. (1990) were therefore considered as atypical. During the last few years, we have extended our chemical, mineralogical, and microstructural study of nodules collected from different sediment types (siliceous ooze, red clay, terrigenous and transition zones of siliceous ooze–red clay, terrigenous–siliceous ooze and calcareous ooze–red clay) spread over a large area in the Central Indian Basin to test whether the nodules of our earlier study are really atypical or are representative for this basin.

2. Materials and methods

The ferromanganese nodules were collected by freefall grabs at 30 sites from an area bounded by latitudes 1ºS and 18ºS and longitudes 75.5ºE and 88.5ºE in the Central Indian Basin (Fig. 1). The nodules rested on siliceous ooze, red clay and terrigenous sediment types and in siliceous ooze–red clay, terrigenous–siliceous ooze, and calcareous ooze–red clay transitional zones. In addition, one nodule each from the red clay (14º00′S, 74º02′E) and siliceous ooze (6º00′S, 75º00′E) substrates was also included in this study (Roy et al., 1990). All samples were collected during cruises organized by the National Institute of Oceanography, Goa, under the project ‘Survey for polymetallic nodules in the Central Indian Ocean’. Bulk samples were analyzed for Mn, Fe, Ni, Cu and Co by a double beam AAS (Perkin Elmer 5000 PE) following standard procedures of sample preparation and using USGS A-1 nodule standard. Electron microprobe line scan analysis of a red clay-hosted nodule (RMS; 14º00′S, 74º02′E) from rim to core was carried out using a JEOL-8600 model microprobe at the JEOL Demonstration Centre, Tokyo, by S. Dasgupta. Electron microprobe point analyses of selected mineral constituents of the nodules were carried out by H. Miura at Hokkaido University, Japan, using a JEOL-JXA 733 model EPMA with accelerating voltage of 15 kV, specimen current of 0.02 nA and electron beam diameter between 2 and 5 μm. The standards used were synthetic oxides of Mn, Fe, Ni, Cu, Co and Zn. The data were corrected using the ZAF programme. Gold-coated chip samples of ferromanganese oxides collected from different depth-intervals from rim to core of the nodules were studied by CAMSCAN (Model 330-HCV) SEM at 20 kV and 170 μA. For petrographic study, nodule-halves were fixed in a cold-setting resin and then polished by a Buehler polishing machine. The polished sections were studied by Leitz Orthoplan Pol reflected light microscope with magnifications ranging from 100× to 1250×. The optical characteristics of todorokite and vernadite (see Section 4) were standardized by means of X-ray diffraction data (Usui, 1979).

3. Bulk chemical composition

The bulk chemical compositions of the nodules are given in Table 1. To express the bulk chemical compositions of marine ferromanganese deposits in terms of hydrogenetic, diagenetic, and hydrothermal compositional fields, Bonatti et al. (1972, 1976) constructed a triangular diagram with Fe, Mn and (Ni + Cu + Co) ×10 as apices. Halbach et al. (1981) slightly modified that diagram adapting it for ferromanganese nodules and used the Mn/Fe ratio as an indicator of hydrogenetic and early diagenetic contributions. These diagrams have been used widely to categorize Fe–Mn nodules into hydrogenetic and early oxic and suboxic diagenetic types. Our data (Table 1) plot on the hydrogenetic and diagenetic fields depending primarily on the Mn/Fe ratios (Fig. 2).

A red clay-hosted nodule (RMS; 14º00′S, 74º02′E), with the bulk composition plotting in the hydrogenetic field (Fig. 2) and consisting of numerous microlayers alternately dominated by todorokite

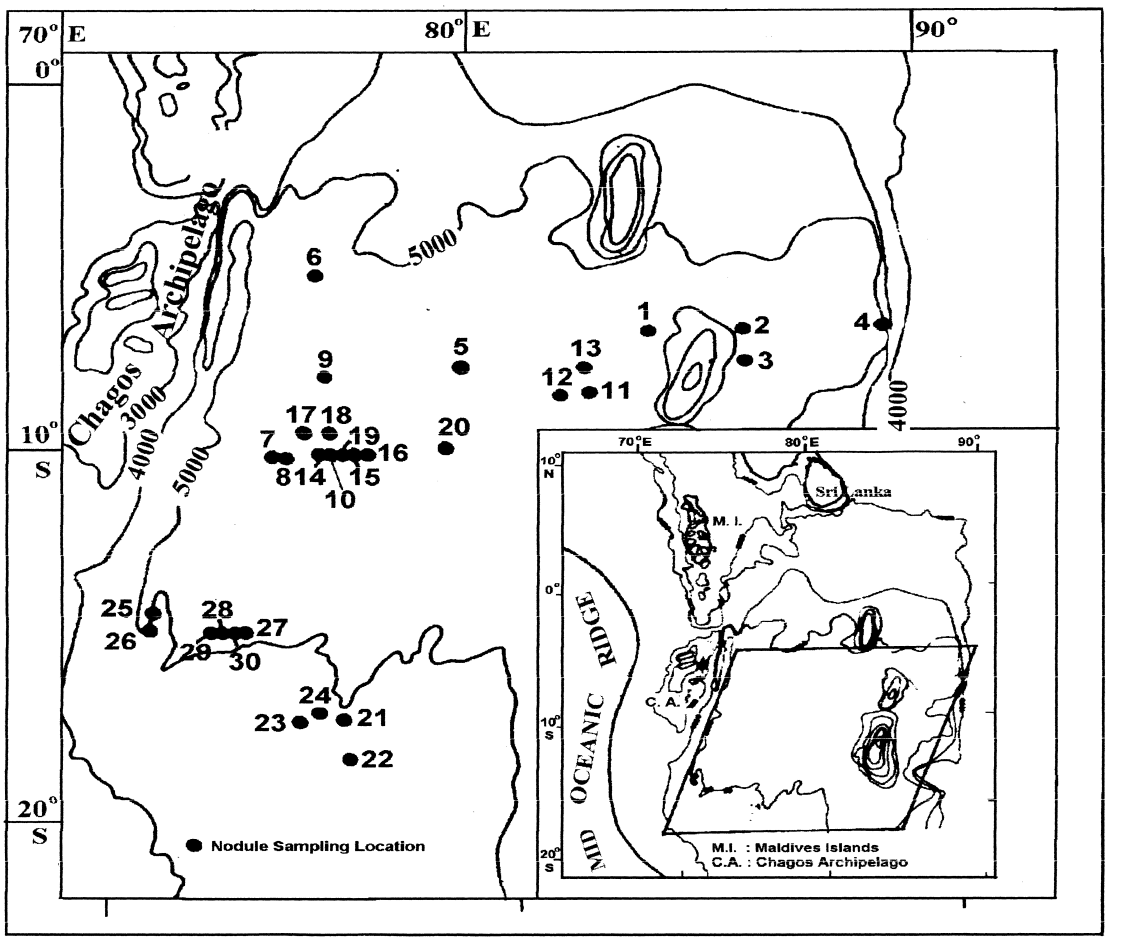

Fig. 1. Location map of studied ferromanganese nodules in the Central Indian Basin, Indian Ocean.

and vernadite (as observed with optical microscope), was subjected to an EPMA line scan from rim to core (Fig. 3). These alternate microlayers yielded contrasting chemical compositions. Todorokite-rich laminae are enriched in Mn, Ni and Cu and depleted in Fe and Co, while the laminae dominated by vernadite show comparative enrichment in Fe and Co. These data indicate covariance of Mn–(Ni + Cu) and Fe–Co in the respective phases. The bulk chemical composition of this nodule therefore represents the weighted average compositions of todorokite- and vernadite-dominated layers. Pacific nodules analyzed by microprobe line scans yielded similar results (Burns and Burns, 1978; Moore et al., 1981). Petrographic examination of CIB nodules also show common mineralogical heterogeneity (todorokite and vernadite) in lamina-scale (see also Halbach et al., 1982; Upenskaya et al., 1987). Both minerals occur as original phases (early diagenetic: todorokite; hydrogenetic: vernadite) but the abundance of todorokite increased during post-depositional diagenesis because of partial conversion of vernadite to todorokite.

We are concerned with the grouping of Ni + Cu + Co in one apex of the diagram as Ni and Cu vary antipathetically to Co with the cumulative effect of a self-cancellation of the influence of the two inverse variables. The diagram then fails to discriminate between the well-established inverse relationship between Ni + Cu (preferentially taken up by todorokite; Burns et al., 1983, 1985) and Co (preferentially admitted in vernadite; Burns, 1965,

Table 1
Partial bulk composition of ferromanganese nodules hosted in different sediment substrates

	Mn	Fe	Ni	Cu	Co
T 1	20.5	9.14	0.71	0.44	0.14
T 2	19.5	9.14	0.65	0.48	0.12
T 3	17.5	10.4	0.48	0.33	0.11
T 4	21.5	7.83	0.74	0.61	0.11
TS 1	19.8	13.5	0.34	0.19	0.19
TS 2	11.9	12.6	0.61	0.51	0.08
TS 3	17.8	9.57	0.64	0.43	0.09
TS 4	19.8	13.1	0.14	0.20	0.16
TS 5	24.1	4.79	1.02	1.01	0.09
TS 6	20.8	8.27	0.72	0.49	0.13
S 1	26.1	3.92	1.05	0.96	0.07
S 2	26.1	3.05	1.08	0.90	0.05
S 3	22.1	6.96	0.89	0.67	0.09
S 4	26.4	3.92	1.16	0.99	0.06
S 5	23.4	4.35	1.10	0.76	0.07
S 6	23.8	5.66	1.04	0.82	0.07
S 7	25.7	3.48	1.24	0.99	0.05
S 8	22.4	5.66	1.00	0.78	0.09
S 9	24.4	6.53	1.02	0.78	0.10
R 1	21.5	10.4	0.51	0.18	0.21
R 2	20.6	11.0	0.54	0.22	0.22
R 3	24.5	7.93	0.86	0.43	0.17
R 4	24.9	7.63	0.82	0.46	0.15
CR 1	28.1	5.19	1.10	0.94	0.09
CR 2	27.7	5.80	1.08	0.78	0.10
SR 1	25.7	7.02	0.94	0.54	0.16
SR 2	27.5	6.71	1.10	0.67	0.13
SR 3	27.5	5.49	1.05	0.79	0.11
SR 4	23.4	9.46	0.80	0.38	0.16
RMS	20.6	11.7	0.69	0.75	0.12

All analyses are given as percentages. Host sediments: T = Terrigeneous sediments; TS = Terrigenous–siliceous ooze sediments; S = Siliceous ooze sediments; R = Red clay; CR = Calcareous ooze–red clay sediments; SR = Siliceous ooze–red clay sediments; RMS = Red clay hosted at 14°00′S 74°02′E.

1976 or vernadite–Fe oxyhydroxide combine). We therefore used a series of binary diagrams to discriminate between the genetic types, one of which is presented here (Fig. 4).

The plots of Mn + Ni + Cu versus Fe + Co (Fig. 4) and Mn versus Fe show negative correlations ($r = 0.8$) because todorokite is comparatively enriched in Mn (and Ni + Cu) and depleted in Fe(+ Co). We obtained two distinct parallel regression lines with the nodules of terrigenous, siliceous ooze and terrigenous–siliceous ooze sediment substrates falling on one line and the siliceous ooze–red clay, red clay and calcareous ooze–red clay-hosted nodules falling on another. In the former group, a general increase in the degree of diagenetic influence from terrigenous to siliceous ooze via terrigenous–siliceous ooze sediment-hosted nodules is apparent. In the latter group, nodules hosted in red clay show the least effect of diagenesis which is consistent with the low permeability of this sediment type (Ericson and Wollin, 1973; Roy et al., 1990). A negative correlation between Mn/Fe ratio and Co ($r = -0.6$) also exists as does a positive correlation between Mn/Fe ratio and (Ni + Cu) ($r = 0.7$). These trends correlate with changes in the todorokite content (and therefore the influence of diagenesis). There is broadly an antipathic relation between (Ni + Cu) and Co ($r = -0.8$), which again correlates with the abundance of todorokite and vernadite.

4. Mineralogy

The mineralogy of these ferromanganese nodules was studied by X-ray diffraction and 10Å manganate (todorokite/buserite) and vernadite (δ-MnO_2) were identified. It was not possible to establish whether todorokite and/or buserite (both reported from marine nodules) represent the 10Å manganate phase by XRD alone (cf. Burns et al., 1985). This phase is referred to as todorokite in the text in view of its more common usage and possibly greater abundance in marine nodules. Electron microprobe spot analyses show that todorokite (nos. 1–6; Table 2) has high Mn/Fe ratios and low Co contents whereas vernadite invariably shows much lower Mn/Fe ratios and higher concentration of Co (nos. 7–10; Table 2). These results are consistent with those obtained by the microprobe line scan (Fig. 3). These vernadites can be equated to Fe-vernadite (Ostwald, 1984; Manceau et al., 1992). It has been suggested that iron is present as feroxyhyte in a fine-scale admixture or epitaxial intergrowth with vernadite (Burns and Burns, 1979; Ostwald, 1984; Manceau et al., 1992). The substantial contents of silica and alumina probably indicate the presence of finely intermixed detrital phases.

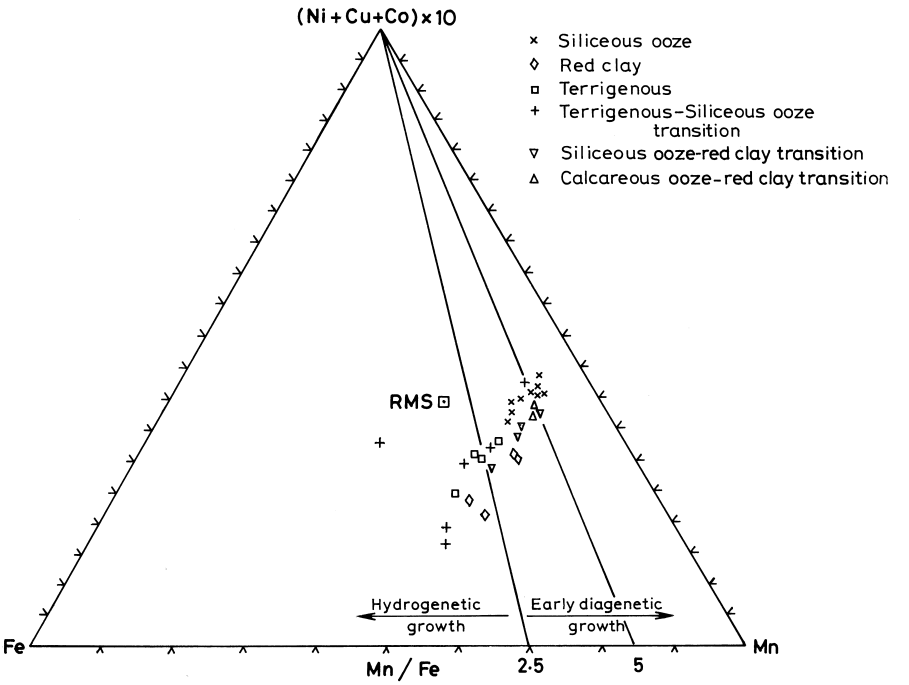

Fig. 2. Partial bulk chemical compositions of ferromanganese nodules from siliceous ooze, red clay, terrigenous, terrigenous–siliceous ooze, siliceous ooze–red clay, and calcareous ooze–red clay sediment types plotted in the Fe–Mn–(Ni + Cu + Co) ×10 ternary diagram. The plot of the bulk composition of the nodule (*RMS*) studied by microprobe line scan (Fig. 3) is also shown in the diagram.

5. Microstructure and texture

The microstructures and textures of the Fe–Mn oxides at different depths in the nodules were studied to determine (a) whether the growth of the nodules was continuous and single microlayers are stacked uniformly, (b) if the microstructures are variable, whether this variability is pervasive or related to specific depths, (c) the state of preservation and dissolution of the biogenic debris incorporated during different stages of primary nodule growth and their possible controls on the evolution of the microstructures, and (d) the nature of post-depositional modifications of mineralogy and microstructures within the nodules. The types of microstructures do not vary much in nodules from different sediment provinces though the biogenic remains in them do show variable abundance and are maximum in nodules from siliceous ooze and minimum in those from terrigenous and red clay sediments. Nodules from transitional terrigenous–siliceous ooze and siliceous ooze–red clay sediment substrates show intermediate concentrations of biogenic remains.

5.1. Primary microstructures

Primary microstructures in the nodules generally remain unmodified down to a depth of ~2 mm from the surface. These are dendritic (Halbach et al., 1981; = columnar/cuspate), laminated (= parallel), and globular (= nondirectional, cf. Heye, 1978; or mottled) types. Multiple microstructural types are present in all nodules irrespective of host sediment types and these occasionally interfere with or merge into one another. Microstructural unconformities suggest depositional hiatuses (Fig. 5a) caused by interim erosion and/or nondeposition. Such growth hiatuses have also been reported to occur in Pacific nodules (Sorem and Fewkes, 1977, 1979), although the ages of these hiatuses remain unknown. Episodic growth and variation in accretion rates of nodules have also been detected in some radiomet-

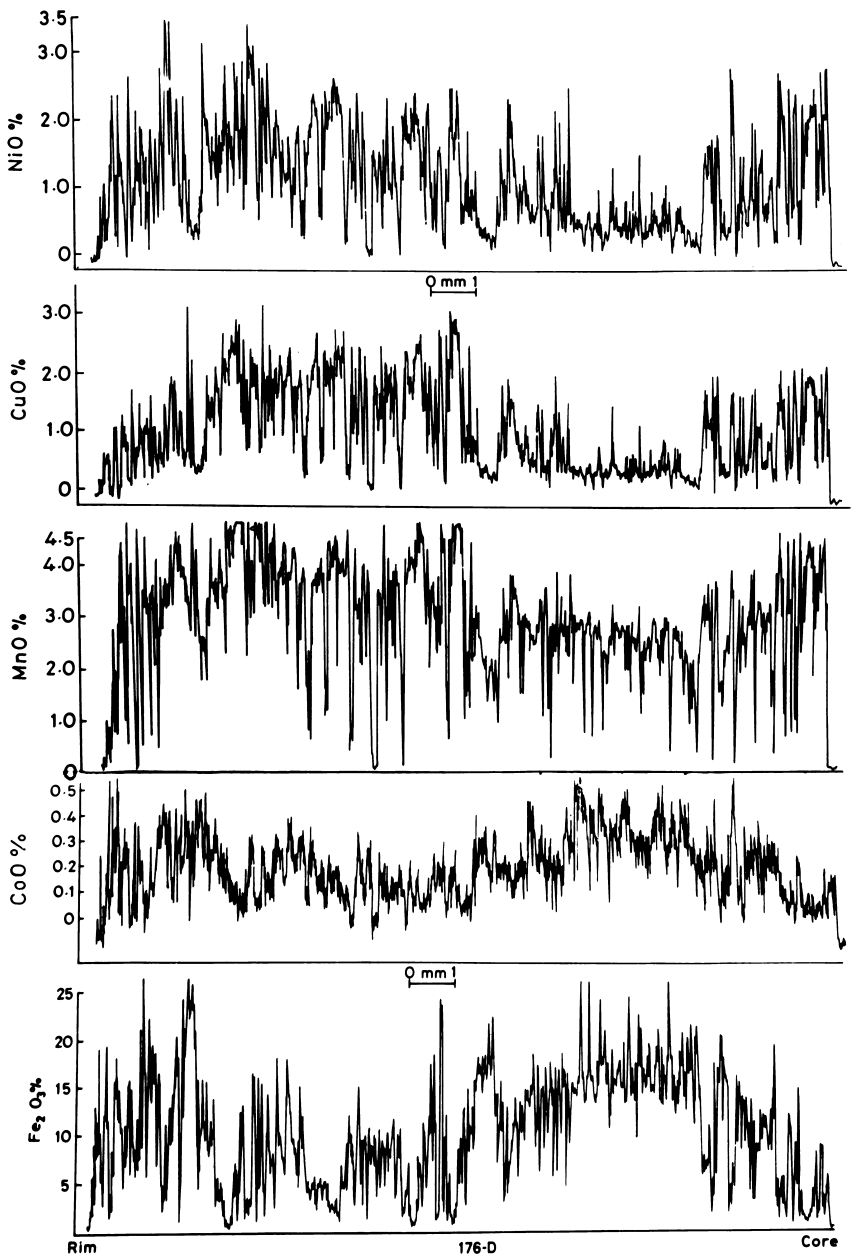

Fig. 3. Electron microprobe line scan from rim to core of a ferromanganese nodule (*RMS* in Fig. 2) from the surface of red clay sediment.

rically dated nodules (Ku, 1977; Krishnaswami and Cochran, 1978; Krishnaswami et al., 1982).

Surface layers of rough-textured nodules exhibit mainly dendritic microstructures consisting of both todorokite and vernadite. In smooth nodules, laminated microstructure, formed by vernadite with or without todorokite, generally prevails but it may also pass into a dendritic growth pattern (Fig. 5b). Well-preserved radiolaria (*Cycladophora davisinia*) tests and diatom frustules are common (Fig. 5c) in the near-surface layers of the nodules that rested on siliceous ooze sediments. Biogenic detritus present

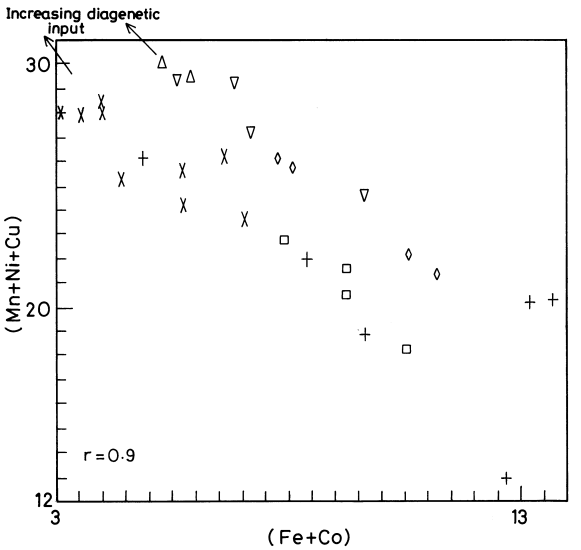

Fig. 4. Covariance of (Mn + Ni + Cu) (%) against (Fe + Co) (%) in the nodules from terrigenous, red clay, siliceous ooze, terrigenous–siliceous ooze, siliceous ooze–red clay, and calcareous ooze–red clay sediment types in two parallel trends indicating diagenetic influence. Symbols as in Fig. 2.

within the nodules frequently acted as substrate for deposition of Fe–Mn oxides forming primary globular microstructures (Fig. 5d). These microstructures were also formed by colloform growth. Such globular growths occasionally punctuate or are overgrown by dendritic microstructures (Fig. 5e). Detrital mineral-rich laminae are concordant with the primary Fe–Mn oxide laminations or they disrupt the latter (Fig. 5f). Microlayers are generally discrete but commonly lack lateral continuity. Sheafs of microlayers usually show a single type of microstructure although in places different types are intermixed rendering the primary growth pattern complex.

The universal validity of the widely followed assumption that todorokite-bearing dendritic microstructure in nodules was developed exclusively by early diagenetic process (Halbach et al., 1981; Marchig and Halbach, 1982) at a rate faster than that for hydrogenetic laminated microstructure (Moore et al., 1981) was questioned (Roy et al., 1990). Dendritic, laminated, and globular microstructures can be either hydrogenetic or early diagenetic. This is further demonstrated by their presence in hydrogenetic ferromanganese crusts developed on volcanic seamounts where the absence of sediment substrates virtually precludes the possibility of early diagenetic metal supply (Segl et al., 1989; Ingram et al., 1990; Hein et al., 1992). These crusts consist mainly of vernadite, rarely with minor todorokite. Variations in the microstructures of these hydrogenetic crusts are thought to be related to changes in bottom current activity and growth rate under changing oceanographic conditions. Faster growth rates have been ascribed to increased bottom water velocity (Segl et al., 1984, 1989). Application of those conclusions to the microstructural characteristics in nodules is still at an initial stage (Banakar et al., 1993) and may be problematic since the nodules resting on sediments have mostly developed by complex processes involving dual sources (hydrogenetic and early diagenetic) at random intervals and possibly at unequal rates. In

Table 2
Electron microprobe analyses of Mn-rich minerals in nodules

	1	2	3	4	5	6	7	8	9	10	11	12
Al_2O_3	3.27	1.79	2.65	1.15	0.29	1.05	3.07	2.81	3.13	3.61	4.16	2.21
SiO_2	9.54	1.38	5.59	1.82	1.07	5.17	7.99	6.31	6.64	8.35	5.39	4.96
MnO_2 [a]	38.1	47.9	41.3	41.6	68.0	59.4	34.8	38.2	34.7	34.7	47.5	30.3
Fe_2O_3 [b]	1.51	0.56	4.63	3.33	0.35	0.83	14.6	14.6	15.4	17.0	8.07	9.04
Co_3O_4	0.07	–	0.12	0.09	–	–	0.81	0.62	0.60	0.63	0.25	0.32
Ni_3O_4	2.38	2.87	2.10	2.52	0.20	0.47	0.71	0.71	0.64	0.59	2.12	1.14
CuO	0.98	1.52	0.88	0.95	0.37	0.56	0.41	0.43	0.45	0.32	1.20	0.29
ZnO	0.21	0.28	0.14	0.08	0.18	0.30	0.16	0.07	0.12	0.11	0.07	0.06
Mn/Fe	23	77	8	11	179	64	2.16	2.36	2.04	1.85	5.32	3.03

All analyses are given as percentages. Numbers 1–4: primary todorokite. Numbers 5, 6: recrystallized todorokite. Numbers 7–10: Vernadite. Numbers 11, 12: mixed vernadite–todorokite.
[a] Total Mn as MnO_2.
[b] Total Fe as Fe_2O_3.

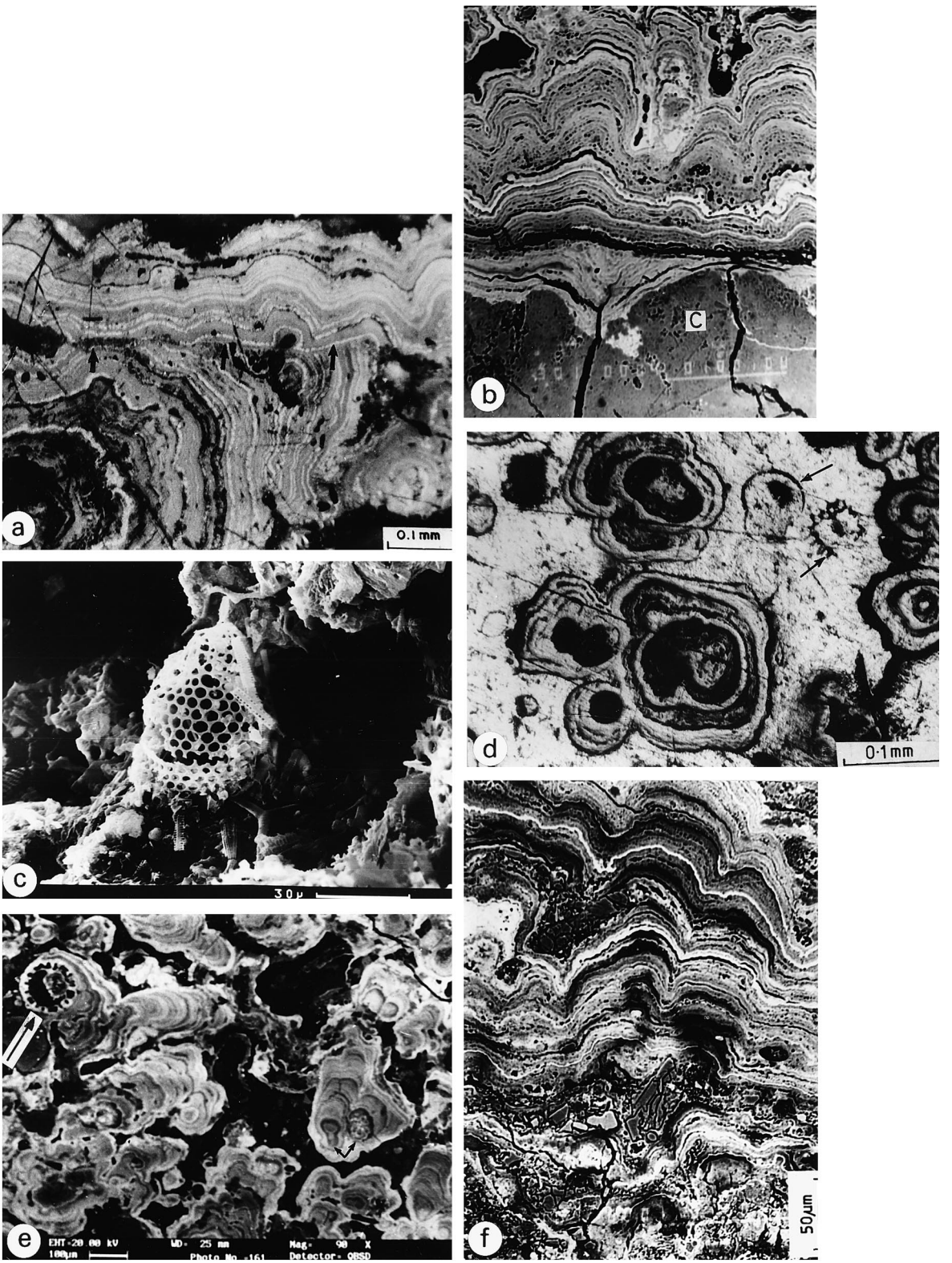
a
0.1 mm
b
c
d
0·1 mm
c
3.0 μ
e
EHT=20.00 kV
100μm
WD= 25 mm
Photo No.=161
Mag= 90 X
Detector= QBSD
f
50μm

addition, even for hydrogenetic crusts, the correlation of specific microstructural types to growth rates remain uncertain (Segl et al., 1984, 1989; Ingram et al., 1990; Hein et al., 1992). The different types of microstructures described in nodules cannot therefore be unambiguously related to growth processes or rates at present.

5.2. Post-depositional features

Evidence of a variety of post-depositional changes in the deeper parts (>2 mm) of the oxide component of the nodules was observed. The most characteristic feature, also recorded in many nodules from elsewhere (Cronan and Tooms, 1968; Sorem and Fewkes, 1977, 1979; Cronan, 1980), is the presence of radial cracks (macroscopic and microscopic) which were formed by post-depositional dehydration (Cronan, 1980; Heath, 1981; Friedrich et al., 1983). These cracks may either be restricted to specific depth zones abutting against younger oxide laminae, indicating internal consolidation of nodule constituents in interim periods of nodule growth, or may cross-cut the entire nodule postdating the nodule growth. The cracks frequently displace primary laminations and are commonly healed by either todorokite (Fig. 6a) or fine-grained unidentified material. Crack infilling took place either from an external source (see also Sorem, 1973; Heye, 1978; Ku and Knauss, 1979) or by internal remobilization.

Fragments of radiolaria and diatom occur at different depth zones of the Fe–Mn oxide layers and these show progressive dissolution with depth. The biogenic remains show evidence of their pseudomorphic replacement by todorokite (Fig. 6b) which possibly indicate simultaneous dissolution of biosilica and precipitation of Mn oxide. On the other hand, phillipsite crystals displaying overgrowths of todorokite formed in the microfossil molds (Fig. 6c) suggesting that both these phases formed as casts of the test walls postdating dissolution of biosilica. Microfossil molds are found to be partially or totally filled with Fe–Mn oxides of a later generation displaying growth patterns that are controlled entirely by the cavity walls (Fig. 6d) and are disharmonious with the surrounding primary microstructures. Therefore dissolution of biogenic remains and precipitation of Mn oxides of a later generation can be both simultaneous and successive. Intranodule diagenesis was modelled by Burns and Burns (1978) involving contribution of metal ions by the dissolving biogenic tests. Kusakabe and Ku (1984) proposed that the biogenic material acted as carrier phases for ^{10}Be and ^{9}Be which released the radionuclides for incorporation to the oxyhydroxide phases on dissolution during post-depositional diagenesis. Both these models may be viable in the above context.

In deeper laminae (>2 mm from the surface), primary cryptocrystalline todorokite has been almost totally recrystallized to coarse grains either around biogenic remains (now molds; Fig. 6e) or in regular microlaminae (Fig. 6f). Electron microprobe point analyses (nos. 1–4, Table 2) show that the Mn content is consistently lower and the Ni and Cu contents higher in the primary todorokite than in the recrystallized grains (nos. 5 and 6, Table 2). This indicates diagenetic redistribution of the elements (see also Roy et al., 1990). In these deeper laminae, todorokite formed at the expense of vernadite as observed with the optical microscope (Fig. 7a). This observation is in accord with that of Roy et al. (1990) but is opposed to the ageing sequence of these two phases

Fig. 5. (a) Growth hiatus within a nodule marked by truncation of earlier interlaminations of todorokite (light grey) and vernadite (dark grey) followed by development of laminations of the same minerals on the plane of erosion/nondeposition (indicated by arrows) (reflected light, oil immersion). (b) Laminated microstructure at the contact with the core (*C*) of the nodule grades gradually outward into dendritic (botryoidal) microstructure. Both microstructures consist of alternations of vernadite (dark grey) and todorokite (light grey) (reflected light, oil immersion). (c) Undissolved radiolaria (*Cycladophora davisiana*) and diatom frustules retained on the nodule surface (SEM). (d) Globular growth of todorokite (light grey molds) and vernadite (dark grey) around biogenic tests (since dissolved leaving black molds). The matrix is recrystallized todorokite. Arrows indicate traces of biogenic tests infilled by oxides (reflected light, oil immersion). (e) Growth of interlaminated todorokite (light grey) and vernadite (dark grey) around pre-existing biogenic tests (now molds; arrows) merging into dendritic microstructures with random growth directions (SEM). (f) Detrital mineral grain-rich (dark grey) laminae (concordant; upper part of the figure) disrupts (lower part of the figure) dendritic microstructure formed by todorokite (light grey) and vernadite (grey) (reflected light, oil immersion).

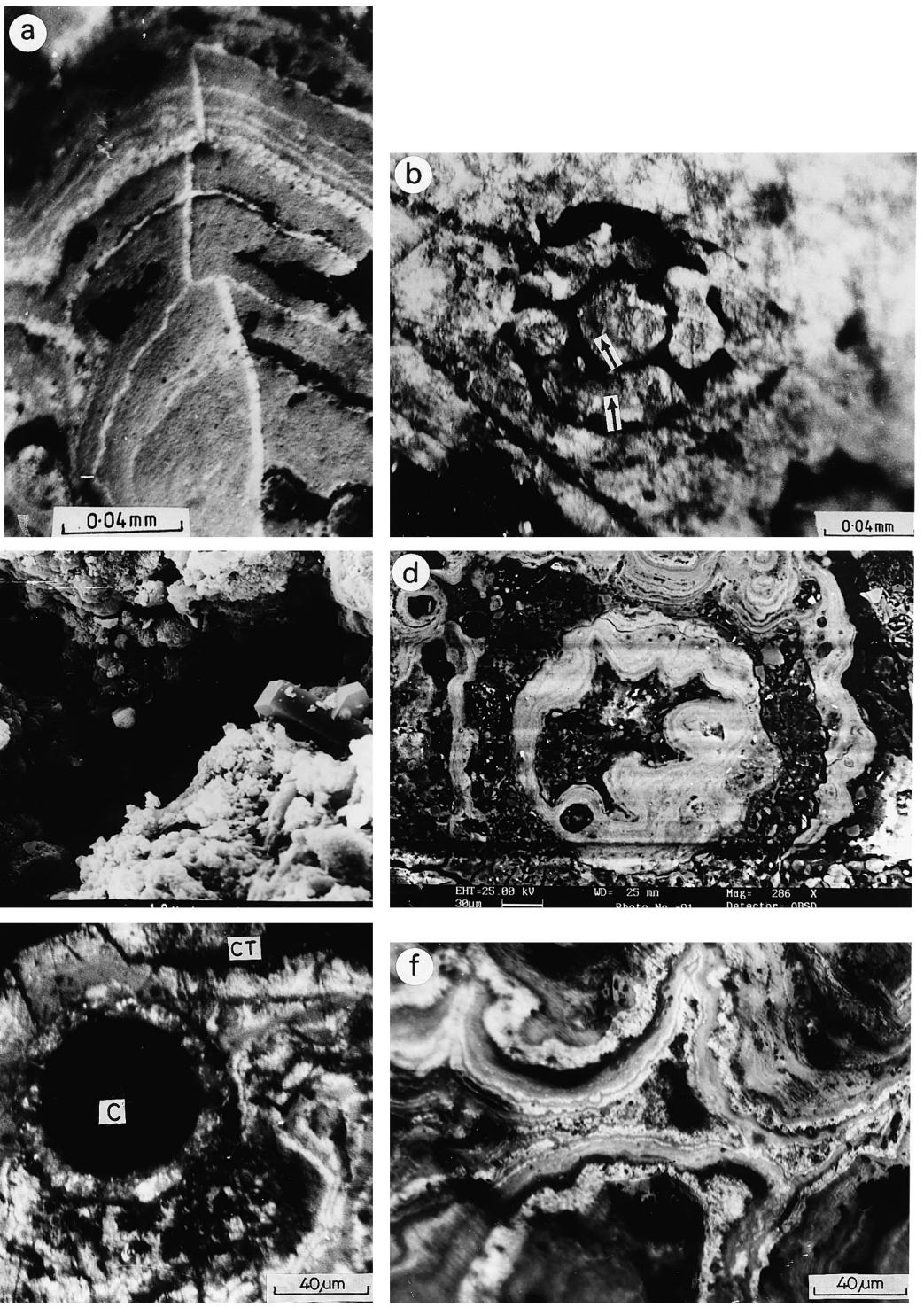
a
0·04mm
b
0·04mm
c
d
EHT=25.00 kV
WD= 25 mm
Mag= 286 X
30µm
e
CT
C
40µm
f
40µm

mentioned by Glasby, 1972 (citing Brooke, 1968). Electron microprobe point analyses of these secondary todorokites, however, yielded compositions (nos. 11 and 12, Table 2) that are intermediate between those characteristic of primary vernadite and todorokite (nos. 1–5 and 7–10, Table 2). This may indicate that the two phases are associated on an extremely fine scale that could not be resolved either optically or by EPMA. Incomplete conversion of vernadite to todorokite (cf. Burns and Burns, 1978) is probable but can not be proved. Late diagenetic todorokite, infilling cross-cutting fractures often swelled forming pods and reducing the primary laminations to a chaotic arrangement (Fig. 7b).

6. Summary

The nodules invariably consist of fine-scale laminations of primary todorokite and vernadite which are chemically distinct (Fig. 3 and Table 2). The average compositions and abundances of these phases are reflected in the bulk compositions plotted in the hydrogenetic and diagenetic fields of the Fe–Mn–(Ni + Cu + Co) ×10 ternary diagram. However, the grouping of Ni + Cu + Co at one apex of this diagram fails to take into account the established antipathic relationship of Ni and Cu with Co. Binary diagrams depicting the covariation of Mn + Ni + Cu against Fe + Co and Mn against Fe based on the bulk compositions of nodules from the different sediment types show two parallel regression lines. One of these exhibits a general increase in the degree of diagenesis in the nodules from terrigenous to siliceous ooze via terrigenous–siliceous ooze sediments while the other shows the same trend in nodules from red clay to siliceous ooze–red clay and calcareous ooze–red clay. These trends of increasing diagenesis are in accord with the increase in biogenic constituents. The nodules resting on siliceous ooze (and its mixture with other sediment types) show higher abundances of biogenic components that, on dissolution, primarily controlled the chemical readjustment during post-depositional diagenesis within the individual nodules. Nodules on a biogenic sediment surface were therefore enriched in todorokite not only through sediment pore water supply but also by post-depositional diagenesis.

Depositional hiatuses confirm that the growth of the oxide layers was not always continuous. The timing of those hiatuses remains unknown.

Primary Fe–Mn oxide laminae are not consistently uniform either in thickness or lateral continuity. Primary microstructures are often complex showing variable patterns, distribution, and interference. Such heterogeneity is attributable to nonuniform growth processes and/or the presence of detritus. Biogenic remains and mineral grains often acted as randomly scattered ‘seeds’ for Fe–Mn oxide deposition producing globular or colloform microstructures that interrupt other primary growth patterns.

The common presence of radial cracks cross-cutting the oxide layers observed here and the high porosity and permeability of the nodules (Han et al., 1979; Cronan, 1980; Mukhopadhyay, 1987; Baturin, 1988) indicate the possibility that the nodules might not be totally closed systems. Post-depositional inward diffusion of radionuclides into nodules (Lalou et al., 1973, 1980; Ku et al., 1979; Huh and Ku, 1984; Kusakabe and Ku, 1984) are in accord with this conclusion. Crack-filling todorokite postdating primary nodule growth could form either through

Fig. 6. (a) Todorokite (light grey) of later generation filling radial cracks cutting across alternating laminations of primary todorokite and vernadite (dark grey) (reflected light, oil immersion). (b) Partial replacement of biogenic tests (black) by todorokite (light grey) associated with clayey matter (dark grey, arrow) (reflected light, oil immersion). (c) Phillipsite crystals (grey) with overgrowths of todorokite (light grey) formed in a test-dissolution cavity. At the right-hand side phillipsite crystals show interpenetrative twin (SEM). (d) Post-depositional cavity infilling by alternating laminae of todorokite and vernadite. These laminations are controlled by cavity walls and are disharmonious with the surrounding primary growth patterns (SEM). (e) Coarsely recrystallized todorokite (light grey) growth around a biogenic test (since dissolved) forming cavity (marked *C*). Note the original control of such biogenic remains on globular microsturcture defined by todorokite (light grey) and vernadite (dark grey) in the left side of the figure. Development of coarse grains of todorokite (*CT*) in the interlaminations on the top right corner of the figure (reflected light, oil immersion). (f) Recrystallization and thickening of todorokite (light grey) laminae alternating with vernadite (dark grey). Note that the recrystallization is more accentuated near the cavities (reflected light, oil immersion).

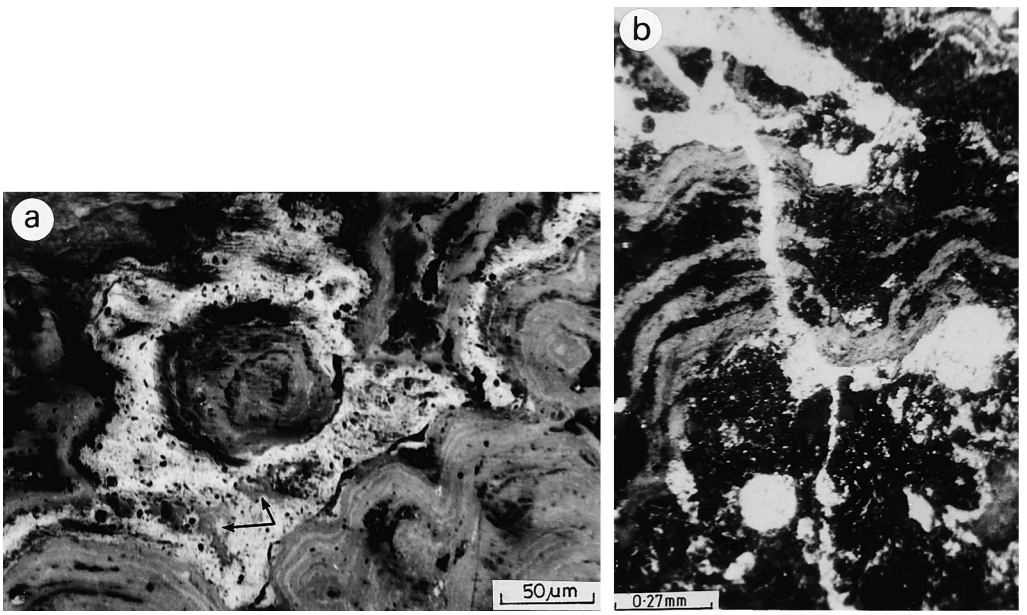

Fig. 7. (a) Advanced stage of conversion of vernadite (dark grey) to todorokite (light grey) with irregular relicts of the former (indicated by arrows) in the latter. Reflected light, oil immersion. (b) Todorokite (light grey) veins cut across primary vernadite (dark grey) laminations forming pods at the ends of veins that chaotically replace the primary microstructures (reflected light, oil immersion).

external supply or by pore water-mediated internal remobilization of metals.

Diagenesis in the deeper (older) part of the oxide layers is indicated by (a) partial pseudomorphic replacement of accreted siliceous biogenic remains by todorokite, (b) almost total dissolution of the biogenic debris followed by growth of phillipsite crystals and later formation of todorokite in the molds, (c) recrystallization of primary cryptocrystalline todorokite (lower Mn and higher Ni and Cu contents) to form coarse grains (higher Mn and lower Ni and Cu contents), (d) possible conversion of vernadite to todorokite, and (e) chaotic disruption of primary laminations by cross-cutting veins of later generation of todorokite. These features suggest the possibilities that either the biogenic tests released transition metals to the pore water on dissolution from which a new generation of oxide phases were produced in their molds or the tests were replaced on a fine scale by the oxides or that both these processes were operative. In any case, the pristine physical and chemical attributes of the nodules in their deeper parts were severely modified (cf. Burns and Burns, 1978). The biogenic (mainly radiolaria and diatom) remains within the nodules are thought to have played a vital role in the compositional changes (including possibly radionuclide) in the internal part of the nodules (cf. Burns and Burns, 1978) since planktons are known to scavenge trace metals during their life cycles (Martin and Knauer, 1973; Boström et al., 1973, 1974, 1978).

Acknowledgements

The authors are grateful to the Director, National Institute of Oceanography, Goa, for providing the nodules collected as part of the programme ‘Surveys for polymetallic nodules in the Central Indian Ocean’ which was supported by the Department of Ocean Development and Council of Scientific and Industrial Research, Government of India. R.B. thanks E. Desa, Director and R.R. Nair, Project Coordinator, N.I.O. for permission to publish this work and for the facilities provided. Thanks are due to S.D. Iyer, S. Chaudhuri, P. Dutta, S. Shome, S. Ghose, U.K. Bhui, G. Parthivan, and S. Jai Shankar for their help at different stages of the work. The manuscript was critically read by A. Mookherjee and P. Sengupta. The critical and constructive reviews by J.R. Hein

and G.P. Glasby have improved the paper considerably. S.R. and S.M. are grateful to the CSIR for financial support. S.R. completed this work during his tenure as INSA Senior Scientist and acknowledges the Indian National Science Academy for financial support. This is N.I.O. contribution No. 2592.

References

Banakar, V.K., Nair, R.R., Tarkian, M., Haake, B., 1993. Neogene oceanographic variations recorded in manganese nodules from the Somali Basin. Mar. Geol. 110, 393–402.

Baturin, G.N., 1988. The Geochemistry of Manganese and Manganese Nodules in the Ocean. Reidel, Dordrecht, Boston, 342 pp.

Bonatti, E., Kraemer, T., Rydell, H.S., 1972. Classification and genesis of submarine iron-manganese deposits. In: Horn, D.R. (Ed.) Ferromanganese Deposits on the Ocean Floor. Natl. Sci. Found., Washington, D.C., pp. 159–166.

Bonatti, E., Zerbi, M.R., Rydell, H.S., 1976. Metalliferous deposits from the Apennine ophiolites: Mesozoic equivalents of modern deposits from oceanic spreading centres. Geol. Soc. Am. Bull. 87, 83–94.

Boström, K., Kraemer, T., Gartner, S., 1973. Provenance and accumulation rates of opaline silica, Al, Ti, Fe, Mn, Cu, Ni, and Co in Pacific pelagic sediments. Chem. Geol. 11, 123–148.

Boström, K., Joensuu, O., Brohm, I., 1974. Plankton: its chemical composition and its significance as a source of pelagic sediments. Chem. Geol. 14, 255–271.

Boström, K., Lysen, L., Moore, C., 1978. Biological matter as a source of authigenic matter in pelagic sediments. Chem. Geol. 23, 11–20.

Burns, R.G., 1965. Formation of Co(III) in the amorphous $FeOOH{\cdot}nH_2O$ phase of manganese nodules. Nature 205, 999.

Burns, R.G., 1976. The uptake of cobalt into ferromanganese nodules, soils and synthetic manganese (IV) oxides. Geochim. Cosmochim. Acta 40, 95–102.

Burns, R.G., Burns, V.M., 1979. Manganese oxides. In: Burns, R.G. (Ed.), Marine Minerals. Mineral. Soc. Am. Short Course Notes 6, 1–46.

Burns, R.G., Burns, V.M., Stockman, H.W., 1983. A review of the todorokite–buserite problem: implications to the mineralogy of marine manganese nodules. Am. Mineral. 68, 972–980.

Burns, R.G., Burns, V.M., Stockman, H.W., 1985. The todorokite–buserite problem: further considerations. Am. Mineral. 70, 205–208.

Burns, V.M., Burns, R.G., 1978. Post-depositional metal enrichment processes inside manganese nodules from the north equatorial Pacific. Earth Planet. Sci. Lett. 39, 341–348.

Cronan, D.S., 1980. Underwater Minerals. Academic Press, London, 362 pp.

Cronan, D.S., Tooms, J.S., 1968. A microscopic and electron probe investigation of manganese nodules from the northwest Indian Ocean. Deep-Sea Res. 15, 215–223.

Ericson, D.B., Wollin, G., 1973. Precipitation of manganese oxide in deep-sea sediments. In: Inter-University Program of Research on Ferromanganese Deposits of the Ocean Floor: Phase I Report. Natl. Sci. Found., Washington, D.C., pp. 99–103.

Friedrich, G., Glasby, G.P., Thijssen, T., Plüger, W.L., 1983. Morphological and geochemical characteristics of manganese nodules collected from three areas on an equatorial Pacific transect by R.V. Sonne. Mar. Min. 4, 167–253.

Glasby, G.P., 1972. The mineralogy of manganese nodules from a range of marine environments. Mar. Geol. 13, 57–72.

Halbach, P., Scherhag, C., Hebisch, U., Marchig, V., 1981. Geochemical and mineralogical control of different genetic types of deep-sea nodules from the Pacific Ocean. Miner. Deposita 16, 59–64.

Halbach, P., Giovanoli, R., Von Borstel, D., 1982. Geochemical processes controlling the relationship between Co, Mn and Fe in the early diagenetic deep-sea nodules. Earth Planet. Sci. Lett. 60, 226–236.

Han, K.N., Hoover, M.P., Fuerstenau, D.W., 1979. The effect of temperature on the physico-chemical characteristics of deep-sea manganese nodules. Mar. Min. 2, 131–149.

Heath, G.R., 1981. Ferromanganese nodules of the deep-sea. Econ. Geol. 75, 736–765, Anniv. Vol..

Hein, J.R., Bohrson, W.A., Schulz, M.S., Noble, M., Clague, D., 1992. Variations in the fine-scale compositions of a Central Pacific ferromanganese crust: paleoceanographic implications. Palaeoceanography 7, 63–77.

Heye, D., 1978. The internal microstructure of manganese nodules and their relationship to the growth rate. Mar. Geol. 26, 56–66.

Huh, C.-A., Ku, T.L., 1984. Radiochemical observations on manganese nodules from three sedimentary environments in the north Pacific. Geochim. Cosmochim. Acta 48, 2187–2193.

Ingram, B.L., Hein, J.R., Farmer, G.L., 1990. Age determinations and growth rates of Pacific ferromanganese deposits using strontium isotopes. Geochim. Cosmochim. Acta 54, 1709–1721.

Krishnaswami, S., Cochran, J.K., 1978. Uranium and thorium series nuclides in oriented ferromanganese nodules: growth rates, turnover times and nuclide behaviour. Earth Planet. Sci. Lett. 40, 45–62.

Krishnaswami, S., Mangini, A., Thomas, J.H., Sharma, P., Cochran, J.K., Turekian, K.K., Parker, P.D., 1982. ^{10}Be and Th isotopes in manganese nodules and adjacent sediments: nodule growth histories and nuclide behaviour. Earth Planet. Sci. Lett. 59, 217–234.

Ku, T.L., 1977. Rates of accretion. In: Glasby, G.P. (Ed.), Marine Manganese Deposits. Elsevier, Amsterdam, pp. 249–267.

Ku, T.L., Knauss, K.G., 1979. Radioactive disequilibrium in fissure filling material and its implication in dating of manganese nodules. In: La Genèse des Nodules de Manganèse. Colloq. Int. C.N.R.S., Paris, pp. 289–293.

Ku, T.L., Omura, A., Chen, P.S., 1979. ^{10}Be and U-series isotopes in manganese nodules from the central north Pacific.

In: Bischoff, J.L., Piper, D.Z. (Eds.), Marine Geology and Oceanography of the Pacific. Plenum Press, New York, pp. 791–814.

Kusakabe, M., Ku, T.L., 1984. Incorporation of Be isotopes and other trace metals into marine ferromanganese deposits. Geochim. Cosmochim. Acta 48, 2187–2193.

Lalou, C., Delibrias, G., Brichet, E., Labeyrie, J., 1973. Existence de carbone-14 au centre de deux nodules de manganèse du Pacifique: ages carbon-14 et thorium-230 de ces nodules. C.R. Hebd. Seance Acad. Sci. Paris 276D, 3013–3015.

Lalou, C., Brichet, E., Bonte, P., 1980. Some new data on the genesis of manganese nodules. In: Varentsov, I.M., Grasselly, G. (Eds.), Geology and Geochemistry of Manganese. Hung. Acad. Sci., Budapest II, pp. 31–90.

Manceau, A., Gorshkov, A.I., Drits, V.A., 1992. Structural chemistry of Mn, Fe, Co and Ni in manganese hydrous oxides: Part II. Information from EXAFS spectroscopy and electron and X-ray diffraction. Am. Mineral. 77, 1144–1157.

Marchig, V., Halbach, P., 1982. Internal structures of manganese nodules related to conditions of sedimentation. Tschermaks Mineral. Petrogr. Mitt. 30, 81–110.

Martin, J.H., Knauer, G.A., 1973. The elemental compositions of plankton. Geochim. Cosmochim. Acta 37, 1639–1653.

Moore, W.S., Ku, T.L., Macdougall, J.D., Burns, V.M., Burns, R.G., Dymond, J., Lyle, M., Piper, D.Z., 1981. Fluxes of metals to a manganese nodule: radiochemical, chemical, structural and mineralogical studies. Earth Planet. Sci. Lett. 52, 151–171.

Mukhopadhyay, R., 1987. Morphological variations in the polymetallic nodules from selected stations in the central Indian Ocean. Geo-Mar. Lett. 7, 45–51.

Ostwald, J., 1984. Ferruginous vernadite in an Indian Ocean ferromanganese nodule. Geol. Mag. 121, 483–488.

Roy, S., Dasgupta, S., Mukhopadhyay, S., Fukuoka, M., 1990. Atypical ferromanganese nodules from pelagic areas of the Central Indian Basin, equatorial Indian Ocean. Mar. Geol. 92, 269–283.

Segl, M., Mangini, A., Bonani, G., Hoffmann, H.J., Nessi, M., Suter, M., Wolfli, W., Friedrich, G., Plüger, W.L., Wiechowski, A., Beer, J., 1984. ^{10}Be-dating of a manganese crust from central North Pacific and implications for ocean palaeocirculation. Nature 309, 540–543.

Segl, M., Mangini, A., Beer, J., Bonani, G., Suter, M., Wolfli, W., 1989. Growth rate variation of manganese nodules and crusts induced by palaeoceanographic events. Palaeoceanography 4, 511–530.

Sorem, R.K., 1973. Manganese nodules as indicators of long-term variations in sea floor environment. In: Morgenstein, M. (Ed.), The Origin and Distribution of Manganese Nodules in the Pacific and Prospects for Exploration. Hawaii Inst. Geophys., Honolulu, pp. 151–164.

Sorem, R.K., Fewkes, R.H., 1977. Internal characteristics. In: Glasby, G.P. (Ed.), Marine Manganese Deposits. Elsevier, Amsterdam, pp. 141–183.

Sorem, R.K., Fewkes, R.H., 1979. Manganese Nodules: Research Data and Methods. Plenum Press, New York, 723 pp.

Upenskaya, T.Y., Gorshkov, A.I., Sivtsov, A.V., 1987. Mineralogy and internal structure of Fe–Mn nodules from the Clarion–Clipperton fracture zone. Int. Geol. Rev. 29, 363–371.

Usui, A., 1979. Nickel and copper accumulation as essential elements in 10Å manganite of deep-sea manganese nodules. Nature 279, 411–413.